Progress In Electromagnetics Research, PIER 92, 181–194, 2009

PREDICTION OF RADOME BORE-SIGHT ERRORS USING A PROJECTED IMAGE OF SOURCE DISTRIBUTIONS

H.-S. Lee

Department of Electronic Engineering
Sogang University
1 Shinsu-dong, Mapo-gu, Seoul, Korea

H. Park

Radar System Group
Samsung Thales
304 Chang-ri Namsa-myeon Young-in Gyoungi-do, Korea

Abstract—In this paper, a calculation method for bore sight error voltage is presented for aperture antennas enclosed in radomes of arbitrary shapes. The method adopts a ray tracing technique frequently used in computer graphics field in constructing two dimensional computer graphics images to obtain a projected image of source distribution, thereby bore sight error voltages and far field radiation patterns are calculated fast and accurately. Besides, the method enables us to use various acceleration schemes used in computer graphics readily. Numerical calculations show that projected source images with a resolution higher than 0.1λ and multiple reflections taken into account produce reliable results. The validity of the method is verified by comparison with results of an analytic solution.

1. INTRODUCTION

A radome is a structure that protects an antenna structure from the outside environment and has been an inevitable component of radars or antenna systems. Although its history is long enough, its analysis is quite cumbersome and time-consuming, because dielectric materials and metal structures coexist. For high frequency approximate

Corresponding author: H.-S. Lee (leehs95@sogang.ac.kr).

solutions, traditional approaches use either physical optics or ray techniques [1–6] such as geometrical optics method, shoot and bouncing method, matrix of pencil method and complex ray methods. The ray method rely on the assumption that curvatures of the radome surfaces are large enough that reflected or transmitted waves can be calculated using Fresnel coefficients of plane interface. These techniques can give accurate results when used in high frequency bands, but their accuracy get worse if the size of radomes shrinks. For enhanced accuracy, the techniques take into account reflections occurred in the radome. Full wave analysis methods are also used such as MOM [7], and FEM [8]. At lower frequency band, these methods yield more accurate results at the expense of hundred or thousand times longer computation time. To shorten the run time, various hybrid methods are devised and fast multipole expansion methods are also applied [9–16]. While these methods give accurate results even at lower frequency range, the long computation time prevents detailed description of radome and antenna structures.

In this paper, we present a ray tracing technique that takes into consideration multiple scattering in the radome comprehensively. This method launches a bundle of rays into grid points on a projection plane for constructing source current images. The images are like the snapshots of antenna surface currents onto a surface that encloses the whole radome and antenna structure. The method resembles a ray technique employed in generating computer graphics images [17] mapped on a surface of solid object except that phase information of the electromagnetic wave as well as amplitude information is utilized for this radome analysis. Because the calculation procedure used in the technique is effectively similar to integrations used in physical optics, it is free from caustic problems. At the same time, it can utilize computer graphics techniques, so that numerous acceleration techniques such as space partitioning and Monte-Carlo methods are imported without paraphrasing. As the density of rays increases or decreases after scattering from dielectric or metallic interfaces according to the radii of curvatures at the scattering points, no separate calculation is needed for the radius of curvature at each scattering point. The method launches a bundle of rays from an observation point to the grid points of a projection plane or a curved surface that surrounds the radome and antenna structure, to find every possible ray path based on geometrical optics from the observation point to the antenna surface currents. The launched rays are split into refracted and reflected rays on each intersection with the radome wall or the antenna structure. The split rays continue to propagate until they hit the region occupied by currents or the number of reflection/refraction

exceeds a predetermined number. In those process, a two dimensional image of a projected source distribution is obtained, of which point source strength is multiplied by phase factors and propagation loss inversely proportional to the traversed distance.

The structure of the article is as follows. In Section 2, a method to transform a current distribution onto other plane is presented. In Section 3, the validity of the formulation is confirmed by comparison with results of an analytic solution, and projected current distributions of a radome enclosed aperture array antenna is shown on a plane and a curved surface. Convergence of the result is also discussed in relation to the resolution of the projected images of current distribution.

2. FORMULATION

Figure 1 shows a radome-enclosed aperture array antenna structure. A typical situation is that an array antenna has tens to hundreds of apertures with radome size tens or hundreds of wavelengths. Traditional approaches use physical optics approximations in which far field electric or magnetic field is obtained via integrating surface currents on the outside radome. The currents are approximated by electric/magnetic field inside the radome multiplied by transmission coefficients at the inner surface point [1–6].

In this formulation of projected source distribution, the electric field outside the radome is obtained using a projected source

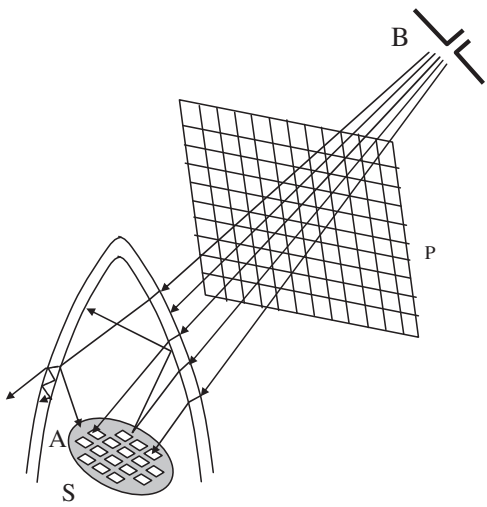

Figure 1. Radome enclosed aperture array antenna.

distribution on the viewing plane P outside the radome structure as shown in Fig. 1, which is the snapshot of the original source distribution on the plane S as is seen from an observation point. The source distribution on the plane P is constructed by casting rays from the observation point into the grid points on the projection plane.

Let us calculate a power received by a dipole antenna 'B' located outside the radome as shown in Fig. 1. Power contributions due to the rays emanating from a radome-enclosed antenna 'A' can be calculated by reciprocity [3]. Reciprocity states that a received power by the antenna 'B' due to a ray through one grid point is the same as the power received by the antenna 'A' due to rays emanating from the antenna 'B' through the same ray paths. For convenience, the projected source distribution on the plane P is calculated with the dipole antenna 'B' as a transmitter and the antenna 'A' as a receiver. It is assumed that the antenna 'B' is an infinitesimally short dipole antenna carrying current $\hat{\mathbf{J}}$ [6]. The incident field by the dipole source is as follows.

$$\mathbf{E}_{in} = -j\omega\mu \left[\hat{\mathbf{J}} - \left(\hat{\mathbf{r}} \bullet \hat{\mathbf{J}}\right)\hat{\mathbf{r}}\right] \frac{e^{-jkr}}{4\pi\, r}, \quad \mathbf{H}_{in} = \frac{\hat{\mathbf{r}} \times \mathbf{E}_{in}}{\eta} \tag{1}$$

where r is the distance from the source to the observation point. μ and η are the permeability and the wave impedance of the free space, respectively.

The rays from the antenna 'B' refract into the radome structure, go on propagating and reflecting on the antenna structure until they are absorbed in apertures, or the number of scattering become larger than a predetermined number. If the ray terminates on hitting the aperture on the antenna 'A', the surface current contribution is added to the projected current at the grid point of the projection plane. The projected current is obtained by multiplying the current on the antenna by a phase factor and the inverse of divergence factor which is the ratio of total traversed distance to the distance from an observation point to the grid point. In calculating the projected source distribution, no consideration of radius of curvature is needed since the ray density varies according to the curvature on the reflection or refraction point.

Figure 2 shows how to obtain a projected source distribution when the radome is absent. A projection plane P is chosen so that the plane covers the source distribution. A bundle of rays are cast into the grid points on the plane, which hit the source distribution. The gridded projection plane helps integrate the source currents. The area of one rectangular grid on the plane P is projected to a magnified area of a rectangle on the surface S whose area is obtained by Eq. (2), where $\cos\theta_P$ is an absolute value of a dot product of the ray direction vector and the normal vector of the plane P at the intersection point on P

and $\cos\theta_S$ is the absolute value of a dot product of the ray direction vector and the normal vector of the plane S at the intersection point on S.

$$\Delta A_i = \left(\frac{R}{r}\right)^2 \frac{\cos\theta_P}{\cos\theta_S}\Delta a \tag{2}$$

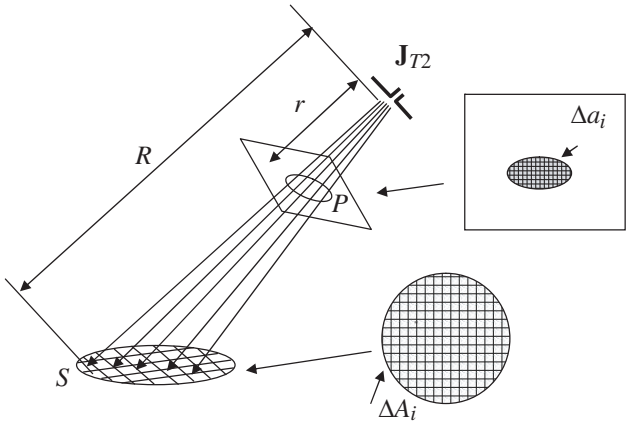

Figure 2. Projected source distribution.

By reciprocity and using Eq. (2), the received power by an array antenna on S is calculated by Eq. (3) which is numerically equally to the received voltage with the dipole antenna current set to unity.

$$\begin{aligned} V = P &= \int_S [\mathbf{J}_M \bullet \mathbf{H}_{in}(\mathbf{r}_S) - \mathbf{J}_E \bullet \mathbf{E}_{in}(\mathbf{r}_S)]dA \\ &= \int_P [\mathbf{J}_M \bullet \mathbf{H}_{in}(\mathbf{r}_P) - \mathbf{J}_E \bullet \mathbf{E}_{in}(\mathbf{r}_P)] \cdot \frac{r}{R} e^{-jk(R-r)} \cdot \left(\frac{R}{r}\right)^2 \left(\frac{\cos\theta_P}{\cos\theta_S}\right) da \\ &= \int_P \left[\mathbf{J}_M^{proj} \bullet \mathbf{H}_{in}(\mathbf{r}_P) - \mathbf{J}_E^{proj} \bullet \mathbf{E}_{in}(\mathbf{r}_P)\right] da \end{aligned} \tag{3}$$

where

$$\mathbf{J}_{M,E}^{proj} = \mathbf{J}_{M,E}\left(\frac{R}{r}\right) \cdot \left(\frac{\cos\theta_P}{\cos\theta_S}\right) \cdot e^{-jk(R-r)}. \tag{4}$$

In Eq. (3), the electric and magnetic field at the point of $\mathbf{r}_S$ of the antenna is replaced by the field at the point $\mathbf{r}_P$ of the projection plane multiplied by divergence and phase factors [18–21].

If a radome encloses the antenna 'A' as shown in Fig. 1, changes occur on ray paths from the antenna 'B' to the antenna 'A'. In the

absence of the radome, the ray paths are straight and one to one correspondence exists for each grid point on the projection plane and a point on the antenna 'A'. However, with the radome, each ray path from the antenna 'B' is split into reflected, transmitted, and diffracted rays on hitting radome surfaces or antenna surfaces [22]. In this formulation, geometrical optics approximation is used to take into account the change in the incident ray and the contribution by diffracted ray is ignored to shorten the calculation time. If a ray hits a smooth metallic surface, only reflection ray is generated. If a ray hits a dielectric interface, it generates both a refracted wave and a reflected wave at the same time. On each scattering mechanisms, electric fields are decomposed into two orthogonal polarization components and are multiplied by reflection or transmission coefficient of each polarization. The resultant electric field is the sum of the two polarizations.

The ray split continues until it hits the region occupied by surface equivalent currents or if the number of reflection/transmission exceeds the predetermined order of reflections. The contribution of a ray through a grid point $\mathbf{r}_P$ on the projection plane to the incident field on the antenna 'A' is obtained by the following Eqs. (5) and (6). Because an incident ray from the transmitter is split into transmit or reflect rays on each scattering, the ray through a grid point $\mathbf{r}_P$ outside the radome impinges on the surface of the radome enclosed antenna at a number of points, which are represented as a sum of split rays.

$$\sum_k \mathbf{E}_{in}(\mathbf{r}_{S,k}) = \left(\sum_k \bar{\mathbf{P}}_k\right) \mathbf{E}_{in}(\mathbf{r}_P) \tag{5}$$

$$\sum_k \mathbf{H}_{in}(\mathbf{r}_{S,k}) = \left(\sum_k \bar{\mathbf{Q}}_k\right) \mathbf{E}_{in}(\mathbf{r}_P) \tag{6}$$

where $\bar{\mathbf{P}}_k$ is a propagation operator accounting for multiple transmissions and reflections occurred in the radome and antenna system that transforms the incident electric field at $\mathbf{r}_P$ on the projection plane into the field impinging on $\mathbf{r}_{S,k}$ of the apertures. $\bar{\mathbf{Q}}_k$ is a transformation operator that converts the incident electric field on the antenna surface into that of magnetic field. They are defined as follows.

$$\bar{\mathbf{P}}_k = \frac{r}{R_k} e^{-jk_0(R_k - r)} \prod_i^{N_k} \left(\bar{\mathbf{T}}_i^k \text{ or } \bar{\mathbf{R}}_i^k\right) \cdot e^{-jk_0(n_i^k - 1)r_i^k}, \tag{7}$$

$$\bar{\mathbf{Q}}_k = \frac{1}{\eta}\left(\hat{\mathbf{r}}_{S,k} \times \bar{\mathbf{P}}\right) \tag{8}$$

where $\bar{\mathbf{T}}_i^k$, $\bar{\mathbf{R}}_i^k$ are dyadic transmission and reflection coefficients of k-th ray leading to the point on the antenna, $\mathbf{r}_{S,k}$, on i-th scattering. r_i^k is the distance from the $(i-1)$-th scattering point to i-th point of k-th ray path. Refractive indices in i-th media is represented as n_i and η is the wave impedance of the free space. The unit vector $\hat{\mathbf{r}}_{S,k}$ represents the incident wave direction on the antenna surface $\mathbf{r}_{S,k}$ after transmissions or reflections. R_k is the total traversed distance from the transmitter and a reception point $\mathbf{r}_{S,k}$. The value r is a distance from the transmitter to a grid point on the projection plane. In calculating transmission or reflection coefficients, it is assumed that intersecting surfaces are locally flat. In Eq. (6), the incident fields at $\mathbf{r}_{S,k}$ on the antenna 'A' are due to the field value at $\mathbf{r}_P$ multiplied by transmission or reflection coefficients and divergence factors of r/R_k. Exhaustive split ray paths can be found using a recursive method commonly used in computer graphics field.

If the radome enclosed antenna is of aperture type and the surface of the antenna is substituted by a perfect magnetic conductor, only magnetic equivalent current generates radiated waves. The induced voltage is obtained by the following Eq. (9).

$$\begin{aligned} V &= \sum_k \int_P \left[2\mathbf{J}_M \bullet \bar{\mathbf{Q}}_k \mathbf{E}_{in}(\mathbf{r}_P)\right] \cdot \left(\frac{R_k}{r}\right)^2 \left(\frac{\cos\theta_P}{\cos\theta_{S,k}}\right) da \\ &= \int_P \mathbf{J}_M \bullet \bar{\mathbf{D}} \mathbf{E}_{in}(\mathbf{r}_P) da = \int_P \left(\bar{\mathbf{D}}^T \mathbf{J}_M\right) da \bullet \mathbf{E}_{in}\left(\mathbf{r}_P\right) \\ &= \int_P \mathbf{J}_E^{proj} \bullet \mathbf{E}_{in}(\mathbf{r}_P) da \end{aligned} \tag{9}$$

where $\bar{\mathbf{D}}^T$ is the transpose of the operator $\bar{\mathbf{D}}$ which is the transformation operator defined as

$$\bar{\mathbf{D}} = 2\sum_k \left(\frac{R_k}{r}\right)^2 \left(\frac{\cos\theta_P}{\cos\theta_{S,k}}\right) \bar{\mathbf{Q}}_k. \tag{10}$$

The transpose operation is equivalent to transforming the magnetic currents on apertures into the electric currents on the projection plane. $\mathbf{J}_E^{proj}$ is a projected current on the plane P and is defined by

$$\mathbf{J}_E^{proj} = \bar{\mathbf{D}}^T \mathbf{J}_M \tag{11}$$

In Eq. (9), an integration on the surface of the antenna 'A' is changed to that on the projection plane P. The projected source distribution can

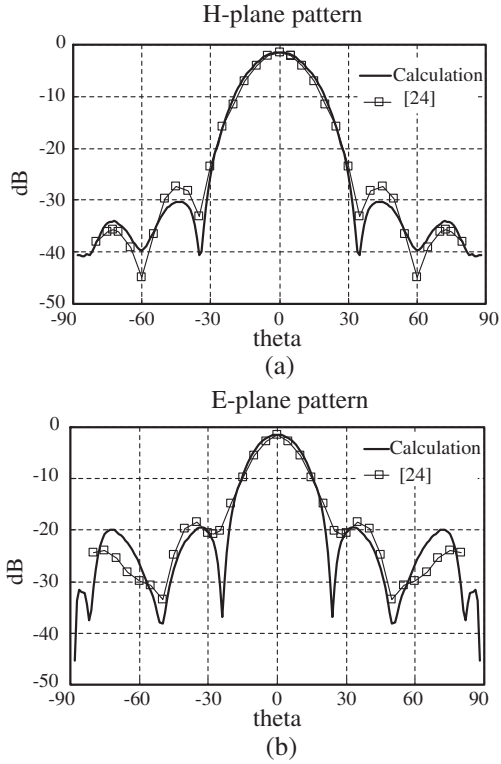

Figure 3. Radiation pattern of a radome enclosed antenna, which has a circular aperture in a hemi-spherical shell radome.

also be obtained using Eqs. (10) and (11). For rapid calculation of the received power, Eq. (9) can be carried out without separately forming the source image, because the image is only a by-product of this formulation. Radiation patterns of co-polar or cross-polar component can be obtained with the dipole antenna current oriented in either co-polar or cross-polar direction.

3. NUMERICAL RESULTS

With the preceding formulation, a computer code is developed for the prediction of radiation patterns or bore-sight error voltages of radome enclosed antennas. As a verification of the validity of the formulation, we compare the radiation pattern of circular aperture antenna enclosed in a radome of which shape is hemi-spherical shell [23, 24]. The radius of the shell is 3λ. Although our formulation ignores diffracted ray paths

and considers reflection and transmission only, the radiation patterns in Fig. 3 show good agreement of our calculation with those of the modal solution.

In this formulation, the projected current distribution is found during the ray tracing process. Fig. 4 shows a projected current

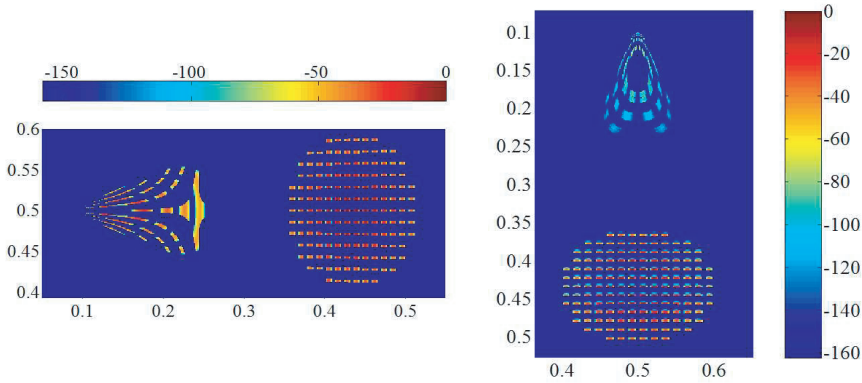

(a) (b)

Figure 4. A strength map of the projected current of a monostatic antenna is drawn on a log scale normalized to the maximum current density. The numbers on the axes are scaled values to the maximum dimensions of the projection plane. (a) Projected current distribution seen from an observation point on H-plane. (b) Projected current distribution seen from an observation point on E-plane.

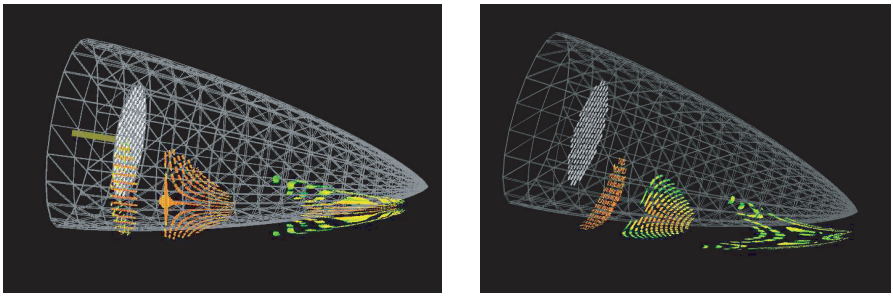

(a) (b)

Figure 5. Projected current formed on a curved surface seen at the angle of 80 degrees from the observation points on the H and E planes. (a) A projected current distribution seen from a point on the H-plane. (b) A projected current distribution seen from a point on the E-plane.

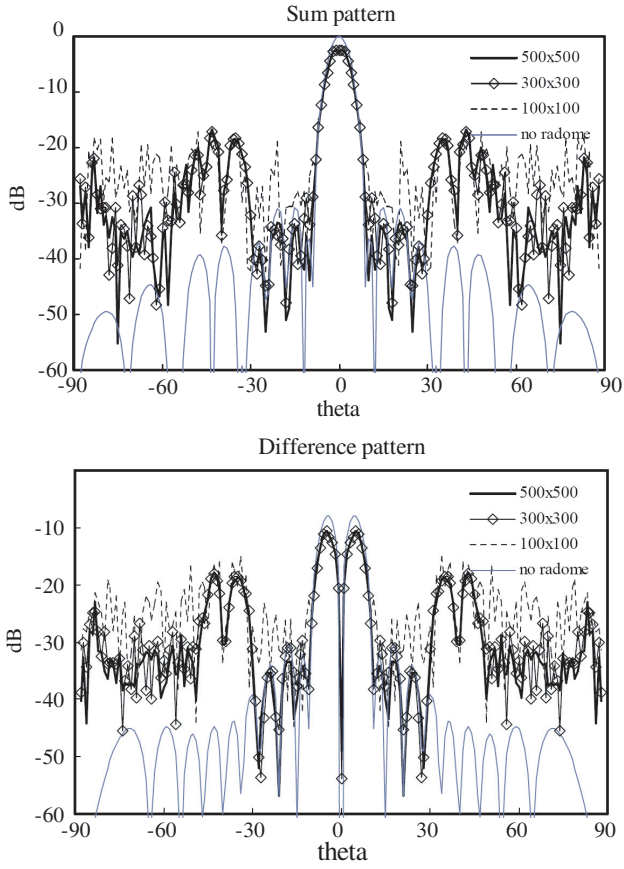

Figure 6. Variations of the radiation patterns (H-plane) with grid sizes. The projection plane is a square with each side 40λ long. "300×300" means that the square is divided into 300×300 squares with sides 0.13λ ($= 40\lambda/300$) long.

distribution of a monostatic antenna as seen from the angle of 40 degree from the main beam direction in the H-plane and the E-plane. In Fig. 4(a), the right side of the current distribution is due to direct rays from the apertures, whereas the left side is due to rays reflected on the radome wall, which should form the image lobe. The radome used in the simulation is of Von Karman shape with a height 32λ (wavelength) and a diameter 16λ with relative permittivity of 2.4. The thickness of the radome is 0.16λ. The array antenna used has 150 apertures. To get an accurate projected surface current distribution,

the projection plane is divided into 600×600 grids. For each grid point, one ray is launched from the receiving dipole antenna. To optimize the calculation time, curved surfaces can be used instead of a rectangle used in Fig. 2. Although the number of rays is large, the time spent is about 15 seconds for a voltage measured at one angle with the reflection order 6 on a PC (Pentium core2duo, 2.4 GHz).

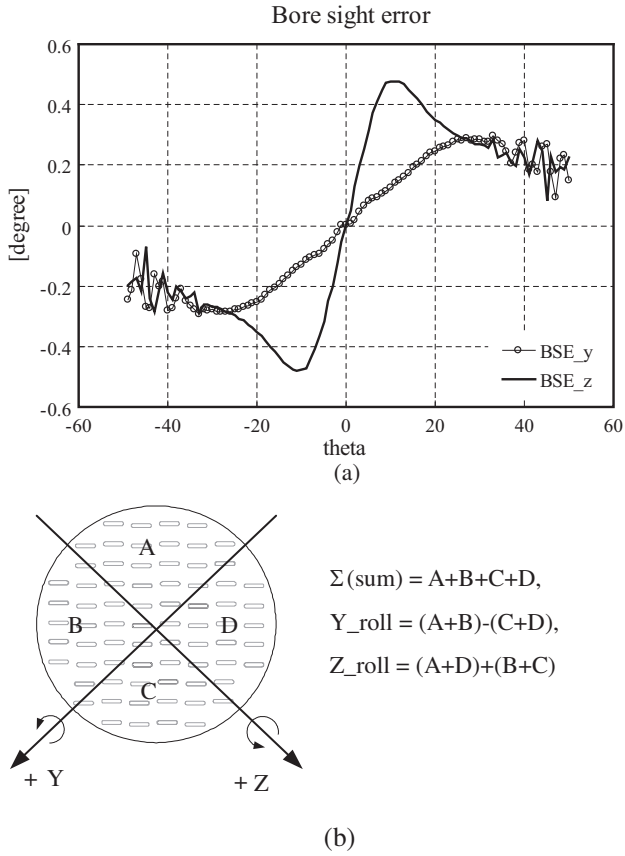

Figure 7. Bore-sight error voltage calculations. (a) BSE voltages calculated with the antenna rotated along the y-roll angles. (b) Aperture distributions and rotation angles.

With a planar projection screen, it is necessary to rebuild grid points whenever a different observation point is chosen. If we adopt a curved projection screen alternatively that encloses the whole radome and antenna structure, we can use the same grid points regardless of different observation points. Fig. 5 shows projected current

distributions on the curved surface. The radome and the aperture antenna used in the simulation is the same as those of Fig. 4.

Figure 6 shows that the calculation result converges if the projection plane is divided into grids which are smaller than about 0.1λ. If the grid size is larger than 0.1λ, the projected current images are obscured by discretization noises which results in errors in the radiation pattern.

The bore-sight error (BSE) voltages can be obtained using the sum and the difference voltages obtained from the monopulse antenna [3]. The voltages are calculated using (9). For each angle, two bore-sight error voltages are calculated with the aperture antenna rotated. In Fig. 7, the BSE angles are calculated with the antenna rotated in z-roll axis. The ripples of BSE at the angle of about 40 degrees are due to the fact that the projected antenna area subtended by each ray increases, which causes discretization noises in the projected current distributions. For each BSE voltage, a projection plane is constructed and rays are launched and traced. The ray tracing is performed using real numbers only and is quickly ended. For the ray only that hits an aperture of the radome enclosed antenna, numerical operations using complex vectors are needed.

4. CONCLUSION

In this paper, a prediction method for bore-sight error voltages is presented. Using a projection plane, the equivalent source current distribution on the radome enclosed antenna is transformed to that on the projection plane. The rays are launched from a receiving antenna into grid points on the plane and are traced until the rays hit the apertures of the antenna or the number of scattering exceeds a predetermined order. For the operations needed, many of the acceleration techniques used in computer graphics fields can be imported, which enables fast calculations. Use of the reciprocity theorem and the inclusion of higher order reflection and transmission enable the simulation results agree with those of a modal solution. Merits of curved projection plane and grid size of the plane are also discussed.

REFERENCES

1. Tricoles, D., "Radiation patterns and boresight error of a microwave antenna enclosed in an axially symmetric dielectric shell," *Journal of the Optical Society of America*, Vol. 54, No. 9, 1094–1101, September 1964.

2. Paris, D. T., "Computer-aided radome analysis," *IEEE Trans. Antennas and Propag.*, Vol. 18, No. 1, 7–15, January 1970.
3. Siwiak, K., T. B. Dowling, and L. R. Lewis, "Boresight errors induced by missile radomes," *IEEE Trans. Antennas and Propag.*, Vol. 27, No. 6, 832–841, November 1979.
4. Burks, D. G., E. R. Graf, and M. D. Fahey, "A high-frequency analysis of radome-induced radar pointing error," *IEEE Trans. Antennas and Propag.*, Vol. 30, No. 5, 947–955, September 1982.
5. Gao, X. J. and L. B. Felsen, "Complex ray analysis of beam transmission through two-dimensional radomes," *IEEE Trans. Antennas and Propag.*, Vol. 33, No. 9, 963–975, September 1985.
6. Orta, R., R. Tascone, and R. Zich, "Performance degradation of dielectric radome covered antennas," *IEEE Trans. Antennas and Propag.*, Vol. 36, No. 12, December 1988.
7. Abdel Moneum, M. A., Z. Shen, J. L. Volakis, and O. Graham, "Hybrid PO-MOM analysis of large axis-symmetric radomes," *IEEE Trans. Antennas and Propag.*, Vol. 49, No. 12, 1657–1666, December 2001.
8. Gordon, R. K. and R. Mittra, "Finite element analysis of axisymmetric radomes," *IEEE Trans. Antennas and Propag.*, Vol. 41, No. 7, 975–981, July 1993.
9. Lu, C.-C., "A fast algorithm based on volume integral equation for analysis of arbitrarily shaped dielectric radomes," *IEEE Trans. Antennas and Propag.*, Vol. 51, No. 3, 606–612, March 2003.
10. Nie, X.-C., Y.-B. Gan, N. Yuan, C.-F. Wang, and L.-W. Li, "An efficient hybrid method for analysis of slot arrays enclosed by a large radome," *Journal of Electromagnetic Waves and Applications*, Vol. 20, No. 2, 249–264, 2006.
11. Pavacic, A. P., D. L. del Rio, J. R. Mosig, and G. V. Eleftheriades, "Three-dimensional ray-tracing to model internal reflections in off-axis lens antennas," *IEEE Trans. on Antennas and Propag.*, Vol. 54, No. 2, 604–612, February 2006.
12. Zou, Y., Q.-Z. Liu, and J. Guo, "Fast analysis of body of revolution radomes with method of moments," *Journal of Electromagnetic Waves and Applications*, Vol. 21, No. 13, 1803–1817, 2007.
13. Oğuzer, T. and A. Altintas, "Free content analysis of the nonconcentric reflector antenna-in-radome system by the iterative reflector antenna and radome interaction," *Journal of Electromagnetic Waves and Applications*, Vol. 21, No. 1, 57–70, 2007.

14. Sukharevsky, O. I. and V. A. Vasilets, "Scattering of reflector antenna with conic dielectric radome," *Progress In Electromagnetics Research B*, Vol. 4, 159–169, 2008.
15. Hemon, R., P. Pouliguen, H. He, J. Saillard, and J. F. Damiens, "Computation of EM field scattered by an open-ended cavity and by a cavity under radome using the iterative physical optics," *Progress In Electromagnetics Research*, PIER 80, 77–105, 2008.
16. Meng, H. F. and W. B. Do, "A hybrid method for the analysis of radome-enclosed horn antenna," *Progress In Electromagnetics Research*, PIER 90, 219–233, 2009.
17. Whitted, T., "An improved illumination model for shaded display," *Communications of the ACM*, Vol. 23, No. 6, 343–349, June 1980.
18. Ling, H., R.-C. Chou, and S.-W. Lee, "Shooting and bouncing rays: Calculating the RCS of an arbitrary shaped cavity," *IEEE Trans. Antennas and Propag.*, Vol. 37, No. 2, 194–2005, Feb. 1999.
19. Liang, C.-H., Z.-L. Liu, and H. Di, "Study on the blockage of electromagnetic rays analytically," *Progress In Electromagnetics Research B*, Vol. 1, 253–268, 2008.
20. Wang, S., H. B. Lim, and E. P. Li, "An efficient ray-tracing method for analysis and design of electromagnetic shielded room systems," *Journal of Electromagnetic Waves and Applications*, Vol. 19, No. 15, 2059–2071, 2005.
21. Chen, C. H., C. L. Liu, C. C. Chiu, and T. M. Hu, "Ultrawide band channel calculation by SBR/Image techniques for indoor communication," *Journal of Electromagnetic Waves and Applications*, Vol. 20, No. 1, 41–51, 2006.
22. Kuroda, S., Y. Inasawa, Y. Konishi, and S. Makino, "Radar cross section analysis considering multi-reflection inside a radome using SBR method," *IEEE APS International Symposium*, Vol. 4, 4503–4506, June 2004.
23. Li, L. W., M. S. Leong, L. Zhou, T. S. Yeo, and P. S. Kooi, "An open-ended circular waveguide with an infinite conducting flange covered by a dielectric hemispherical radome shell: Full wave analysis and Green dyadic," *Progress In Electromagnetics Research*, PIER 21, 221–245, 1999.
24. Li, L. W., M. S. Leong, L. Zhou, T. S. Yeo, and P. S. Kooi, "Improved analysis of antenna radiation from a circular aperture covered by a dielectric hemispherical radome shell," *IEE Proceedings-Microwaves, Antennas and Propagation*, Vol. 147, No. 2, 144–150, April 2000.